Quantum simulation in hybrid transmission lines

Alessandro Ferreri* and Frank K. Wilhelm
Institute for Quantum Computing Analytics (PGI-12), Forschungszentrum Jülich, Jülich 52425, Germany

(Received 2 July 2024; revised 11 December 2024; accepted 24 January 2025; published 10 February 2025)

Platforms based on transmission lines are nowadays employed for the simulation of standard phenomena in quantum electrodynamics and quantum field theory. In this work, we propose a hybrid platform, in which a right-handed transmission line is connected to a left-handed transmission line by means of a superconducting quantum interference device. We examine the interaction between the two transmission lines, as well as the excitation flow along the composite platform. We show that, by activating specific resonance conditions, this platform can be used as a quantum simulator of different phenomena in quantum optics, multimode quantum systems, and quantum thermodynamics.

DOI: 10.1103/PhysRevApplied.23.024026

I. INTRODUCTION

Quantum simulation occupies a pre-eminent role in the development of state-of-the-art quantum technologies for the study of complex quantum phenomena, which could not be investigated via direct observations [1–14]. Nowadays, we can account for a vast range of quantum systems that can be employed as a quantum simulator. Among these systems, particularly successful platforms for implementations in quantum simulation are the superconducting circuits [15–27]. Depending on the arrangement of the circuit elements, these devices can simulate, e.g., two-level systems (qubits), and quantum harmonic oscillators, and for this reason, superconducting circuits find application as quantum simulators of a large number of physical scenarios in quantum electrodynamics (QED) [28–30], atomic physics, and quantum optics [2].

Superconducting electrical circuits are particularly effective for the investigation of multimode quantum systems, such as quantum fields or many-body systems [22, 31,32]. Typical examples are transmission lines (TLs), which well describe (1+1)-dimensional quantum fields either in free space or confined in a resonator [33]. In the last two decades, the solid analogy between TLs and quantum scalar fields, as well as the possibility to externally drive the magnetic flux by means of superconducting quantum interference devices (SQUIDs), was of great support for the investigation of quantum relativistic phenomena, with particular focus on those stemming from the stimulation of the quantum vacuum [34]. For instance, effects of particle creation have been predicted in diverse waveguidelike TLs [35–37]; well-known examples thereof are the dynamical Casimir effect [38–41] (then observed experimentally [3,4]), and the Hawking radiation [42–45].

Continuous transmission lines are normally right handed, meaning that the dielectric constant and the magnetic permeability are both always positive. Due to the right handedness, the dispersion relation of such TLs enables the promotion of the discrete circuit nodes to the continuous limit [28]. However, almost 70 years ago Vaselago proposed left-handed media [46], which are characterized by negative dielectric constant and magnetic permeability; moreover, the wave vector points to the opposite direction with respect to the Poynting vector [47]. As a consequence of the left handedness, in a limited range of frequencies such a metamaterial also responds to the electromagnetic field with a negative refractive index [48,49]. In circuit QED, circuit platforms showing left-handed features in the dispersion relation are called "left-handed transmission lines (LHTLs)" [50–52].

In this work, we present a hybrid platform realized by joining a left-handed and a right-handed transmission line (RHTL) [53–56]. To join the two TLs, we make use of a SQUID. We place this device on the edge between the two TLs, such that it can directly couple the magnetic flux stemming from both TLs. We examine the energy conservation at the SQUID, showing that the interaction between the two TLs leads to an energy-shift term altering the frequency matching between left-handed and right-handed modes. Of note, by tuning the Josephson energy of the SQUID we can externally drive the dynamics of the composite transmission line (CTL). We observe that,

*Contact author: a.ferreri@fz-juelich.de

by properly manipulating the Josephson energy, we can simulate a large spectrum of phenomena described by a linear dynamics (e.g., quantum optics, including nonlinear optics phenomena). Finally, we propose some applications to the engineering of highly entangled states [57,58] and to quantum thermodynamics [59–61].

The paper is structured as follows: in Sec. II we present the CTL and discuss the differences between LHTL and RHTL in terms of dispersion relations and eigenenergies of the Hamiltonian. In Sec. III we address the problem of the energy conservation at the SQUID, and examine the possibility to propagate quanta of magnetic flux fields from one TL to the other one. In Sec. IV we show that the interaction Hamiltonian can display different types of two-mode couplings depending on the activated resonance condition between the Josephson energy and the modes of both the LTHL and the RHTL. We also study the correlation between these modes. In Sec. VI we present different scenarios wherein our CTL can find application as quantum simulator and quantum thermal machine. We conclude in Sec. VII. Starting from basic circuit equations, in Appendix A we mathematically obtain the Hamiltonian from the Lagrangian using the magnetic fluxes as scalar fields, and analyze the single terms of the Hamiltonian of interaction.

II. THEORETICAL BACKGROUND

The hybrid TL is pictorially represented in Fig. 1. It is made up of two different platforms, namely a LHTL and a RHTL, connected together by one SQUID at the edge in between. We assume that the CTL consists of $2N$ identical unit cells, where N is the number of discrete unit cells equal in both the LHTL and RHTL. Each unit cell is characterized by the length unit Δx, determining the minimum wave length for the transmission lines, $\lambda = 2\Delta x$, and confining the wave vector within the first Brillouin zone [54]. The presence of the SQUID with the time-dependent Josephson energy ensures the interaction between the two TLs; furthermore, we will see that it allows to impose the energy conservation for selected modes of the CTL.

The Lagrangian of the hybrid transmission line consists of three parts, two thereof describe the left-handed and the right-handed component individually, whereas the last term is responsible for their interaction:

$$\mathcal{L} = \mathcal{L}_{\mathrm{L}} + \mathcal{L}_{\mathrm{R}} + \mathcal{L}_{\mathrm{I}}, \tag{1}$$

where

$$\mathcal{L}_{\mathrm{L}} = \frac{1}{2}\sum_{n_{\mathrm{l}}=1}^{N}\left[C_{\mathrm{l}}(\dot{\Phi}^{\mathrm{L}}_{n_{\mathrm{l}}+1} - \dot{\Phi}^{\mathrm{L}}_{n_{\mathrm{l}}})^2 - \frac{(\Phi^{\mathrm{L}}_{n_{\mathrm{l}}})^2}{L_{\mathrm{l}}}\right], \tag{2a}$$

$$\mathcal{L}_{\mathrm{R}} = \frac{1}{2}\sum_{n_{\mathrm{r}}=1}^{N}\left[C_{\mathrm{r}}(\dot{\Phi}^{\mathrm{R}}_{n_{\mathrm{r}}})^2 - \frac{(\Phi^{\mathrm{R}}_{n_{\mathrm{r}}+1} - \Phi^{\mathrm{R}}_{n_{\mathrm{r}}})^2}{L_{\mathrm{r}}}\right], \tag{2b}$$

$$\mathcal{L}_{\mathrm{I}} = E(t)\cos\left[\frac{2\pi}{\phi_0}\left(\Phi^{\mathrm{L}}_1 - \Phi^{\mathrm{R}}_1\right)\right]. \tag{2c}$$

In the expressions above, $\Phi^{\mathrm{L}}_{n_{\mathrm{l}}}$ ($\Phi^{\mathrm{R}}_{n_{\mathrm{r}}}$) represents the value of the magnetic flux field of the left-handed (right-handed) transmission line at the position n_{l} (n_{r}), C_{l} and L_{l} are the capacitance and the inductance of the LHTL, whereas C_{r} and L_{r} are the capacitance and inductance of the RHTL, respectively. Note that the higher n_{l} and n_{r}, the farther the labeled position with respect to the SQUID. Finally, $E(t)$ is the time-dependent Josephson energy, and $\phi_0 = \pi\hbar/e$ is the magnetic flux quantum.

For the sake of simplicity, in our description we assume that the capacitance of the Josephson junctions in the SQUID is small with respect to the capacitance at both the LHTL and the RHTL, $C_{\mathrm{J}} \ll C_{\mathrm{l}}, C_{\mathrm{r}}$, implying that we can neglect it in our description. We will work in a regime where $\left(\Phi^{\mathrm{L}}_1 - \Phi^{\mathrm{R}}_1\right)/\phi_0 \ll 1$, namely we make the assumption that the amplitude of the external magnetic flux at the SQUID is much smaller than the magnetic flux quantum [36,39,40,62], thereby writing the interaction Lagrangian as

$$\mathcal{L}_{\mathrm{I}} \simeq -\frac{E(t)}{2}\left(\frac{2\pi}{\phi_0}\right)^2\left(\Phi^{\mathrm{L}}_1 - \Phi^{\mathrm{R}}_1\right)^2. \tag{3}$$

In Eq. (3) we expanded the cosine to the lowest order in $2\pi\left(\Phi^{\mathrm{L}}_1 - \Phi^{\mathrm{R}}_1\right)/\phi_0$, obtaining the quadratic Lagrangian in the classical amplitudes of the field.

Solving the Euler-Lagrange equations far from the SQUID, namely at $1 < n_{\mathrm{l}}, n_{\mathrm{r}} < N$ [54],

$$\begin{aligned} C_{\mathrm{l}}L_{\mathrm{l}}\left(\ddot{\Phi}_{n+1} + \ddot{\Phi}_{n-1} - 2\ddot{\Phi}_n\right) &= \Phi_n, \\ \frac{1}{C_{\mathrm{r}}L_{\mathrm{r}}}\left(\Phi_{n+1} + \Phi_{n-1} - 2\Phi_n\right) &= \ddot{\Phi}_n, \end{aligned} \tag{4}$$

we get the discrete mode expansions of the quantum flux field in both the LHTL and the RHTL in terms of plane wave:

$$\hat{\Phi}^{\mathrm{L}}(n_{\mathrm{l}}, t) = \sum_{|j|=1}^{N/2}\sqrt{\frac{\hbar}{2C_{\mathrm{l}}N\omega_j}}\left(e^{i(k_j n_{\mathrm{l}}\Delta x - \omega_j t)}a_j + \mathrm{h.c.}\right), \tag{5}$$

$$\hat{\Phi}^{\mathrm{R}}(n_{\mathrm{r}}, t) = \sum_{|j|=1}^{N/2}\sqrt{\frac{\hbar}{2C_{\mathrm{r}}N\upsilon_j}}\left(e^{i(p_j n_{\mathrm{r}}\Delta x - \upsilon_j t)}b_j + \mathrm{h.c.}\right), \tag{6}$$

where ω_j and k_j are frequency and wave vector of the left-handed TL, respectively; whereas υ_j and p_j are frequency and wave vector of right-handed TL, respectively. The sum over all modes accounts for plane wave propagating both leftwards (negative sign of j) and rightwards (positive sign of j) along the CTL. Here, a_j and b_j are the classical amplitudes of the LHTL and RHTL magnetic flux

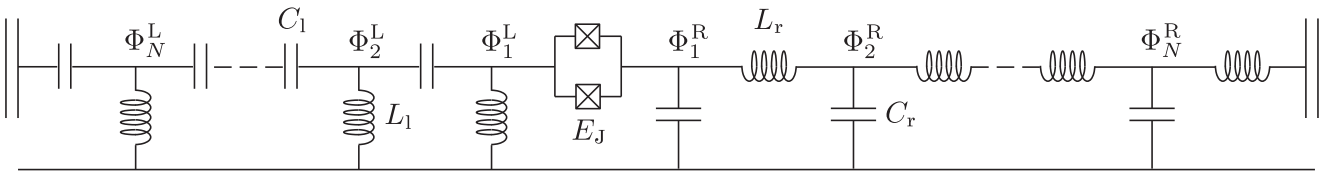

FIG. 1. Schematic representation of the hybrid transmission line. It consists of a left-handed and a right-handed transmission line, each of N unit cells, connected by a SQUID in series.

fields, respectively. By means of the Euler-Lagrange equations, we also find that the two TLs are characterized by the following dispersion relations:

$$\omega_j = \frac{1}{2\sqrt{C_{\mathrm{l}}L_{\mathrm{l}}}\left|\sin\left(\frac{k_j\,\Delta x}{2}\right)\right|}, \tag{7}$$

$$\upsilon_j = \frac{2\left|\sin\left(\frac{p_j\,\Delta x}{2}\right)\right|}{\sqrt{C_{\mathrm{r}}L_{\mathrm{r}}}}, \tag{8}$$

for the LHTL and RHTL, respectively. Note that the form of the wave vectors is identical for both TLs, $w_j = 2\pi j/(N\,\Delta x)$, with $w = k,p$. Referring to Fig. 1, in our notation the positive sign of the wave vectors always indicates the rightwards propagation of the signal.

Before introducing the quantization protocol of the CTL we need to clarify the role of the SQUID as a crucial element for the boundary conditions of the transmission line. The interaction Lagrangian in Eq. (2c) encodes a local time-dependent interaction between the two TLs. To externally drive the interaction, at $t > 0$ we modulate the Josephson energy of the SQUID around a fixed value according to $E(t) = E_0[1 + \eta\cos(\Omega t)]$, where $E_0 = I_{\mathrm{c}}\phi_0$ is the average value of the Josephson energy with critical current I_{c}. Here, Ω and η are the oscillation frequency and the dimensionless oscillation amplitude, respectively. In our formalism we assumed that the oscillation amplitude of the Josephson energy is much smaller than its average value, namely $\eta \ll 1$. By means of this assumption, we can safely state that the frequencies of the magnetic flux field are only weakly affected by the modulation of the Josephson energy (frequency shift effects are described in Sec. III). This perturbative approach allows us to both solve the equation of motion of the field by means of static boundary conditions, and encode the time dependence of the interaction only in the coupling strength of the interaction Lagrangian. Similar perturbative techniques have been employed in other contexts, for example, in cavity optomechanics [63–65].

The quantization of the two classical magnetic flux fields occurs in accord to the standard procedure [51,66]: we first promote the classical fields in Eqs. (5) and (6), as well as the canonical momenta $P^{\mathrm{L}}(n_{\mathrm{l}},t)$ and $P^{\mathrm{R}}(n_{\mathrm{r}},t)$ defined, respectively, in Eqs. (A6) and (A7), to quantum operators: these fulfill the bosonic commutation relation

$$\left[\hat{\Phi}^{\mathrm{L}}(n,t),\hat{P}^{\mathrm{L}}(m,t)\right] = \left[\hat{\Phi}^{\mathrm{R}}(n,t),\hat{P}^{\mathrm{R}}(m,t)\right] = i\hbar\delta_{nm}, \tag{9}$$

whereas all other commutators are equal to zero. The quantization of the classical amplitudes is derived by discrete Fourier transforming Eqs. (5), (6), (A6), and (A7) and exploiting the commutation rule in Eq. (9) [51]. We get

$$\left[\hat{a}_i,\hat{a}_j^\dagger\right] = \frac{\delta_{ij}}{4\sin^2\left(\frac{k_j\,\Delta x}{2}\right)}, \tag{10}$$

for the magnetic flux field in the LHTL and

$$\left[\hat{b}_i,\hat{b}_j^\dagger\right] = \delta_{ij}, \tag{11}$$

for the magnetic flux field in the RHTL. From now on, we will refer to the excitations (or particles) generated in the LHTL as left-handed excitations (LHEs) and to the excitations generated in the RHTL as right-handed excitations (RHEs).

Starting from the Lagrangian in Eq. (1) and the explicit expressions for the two magnetic flux fields written above, we can derive the Hamiltonian $\hat{\mathcal{H}} = \hat{\mathcal{H}}_{\mathrm{L}} + \hat{\mathcal{H}}_{\mathrm{R}} + \hat{\mathcal{H}}_{\mathrm{I}}$, where

$$\hat{\mathcal{H}}_{\mathrm{L}} = 4\hbar\sum_{|j|=1}^{N/2}\omega_j\sin^2\left(\frac{k_j\,\Delta x}{2}\right)\hat{a}_j^\dagger\hat{a}_j, \tag{12}$$

$$\hat{\mathcal{H}}_{\mathrm{R}} = \hbar\sum_{|j|=1}^{N/2}\upsilon_j\hat{b}_j^\dagger\hat{b}_j, \tag{13}$$

constitute the two parts of the noninteracting Hamiltonian for the left-handed and right-handed transmission lines, $\hat{\mathcal{H}}_0 = \hat{\mathcal{H}}_{\mathrm{L}} + \hat{\mathcal{H}}_{\mathrm{R}}$, and

$$\hat{\mathcal{H}}_{\mathrm{I}} = \chi(t)\left\{\sum_{|j|=1}^{N/2}\left[\frac{1}{\sqrt{C_{\mathrm{l}}\omega_j}}\left(e^{-ik_j\,\Delta x}\hat{a}_j^\dagger + e^{ik_j\,\Delta x}\hat{a}_j\right)\right.\right.$$
$$\left.\left. - \frac{1}{\sqrt{C_{\mathrm{r}}\upsilon_j}}\left(e^{-ip_j\,\Delta x}\hat{b}_j^\dagger + e^{ip_j\,\Delta x}\hat{b}_j\right)\right]\right\}^2, \tag{14}$$

with $\chi(t) = \hbar E(t)/2N\,(2\pi/\phi_0)^2$, is the interaction Hamiltonian. The mathematical derivation of the Hamiltonian

is reported in Appendix A. We notice that, as long as we do not account for the interaction at the SQUID, the eigenenergies in Eq. (12) are structurally identical to the eigenvalues (frequencies) in Eq. (13),

$$\epsilon_j \equiv 4\hbar\omega_j \sin^2\left(\frac{k_j\,\Delta x}{2}\right) = \frac{2\hbar\left|\sin\left(\frac{k_j\,\Delta x}{2}\right)\right|}{\sqrt{C_{\rm l}L_{\rm l}}}. \tag{15}$$

Therefore, the bare energy grows with the wave vector up to the border of the first Brillouin zone in both LHTL and RHTL, despite the different structure of the dispersion relations [51].

III. PHASE MATCHING AT THE SQUID

In this section we examine the signal propagation along the CTL. In particular, we want to figure out whether the interaction between two TLs characterized by different dispersion relations enables energy and momentum propagation at their intersection. To address this issue properly, we need to analyze the interaction Hamiltonian in detail.

Once we expand the square in Eq. (14), we observe that the interaction Hamiltonian can be split conveniently into smaller terms, each representing a specific type of two-mode coupling:

$$\hat{\mathcal{H}}_{\rm I} = \hat{\mathcal{H}}_{\rm ES} + \hat{\mathcal{H}}_{\rm HP} + \hat{\mathcal{H}}_{\rm RM} + \hat{\mathcal{H}}_{\rm 1S} + \hat{\mathcal{H}}_{\rm 2S} + \hat{\mathcal{H}}_{\rm IS}. \tag{16}$$

More details about the single contributions of the Hamiltonian in Eq. (16) and their explicit form are discussed in Appendix A. Note that the interaction can occur both within the same TL, and between modes stemming from the left-handed and right-handed components.

We now need to figure out whether all terms of the interaction Hamiltonian contribute to the dynamics with equal weigh, or whether there are resonant terms whose contribution play a major role. To verify this, we momentarily move our description to the interaction picture, and observe if there are static terms in the Hamiltonian. Once we move to the interaction picture, the only constant term in the interaction Hamiltonian is

$$\hat{\mathcal{H}}^{\rm I}_{\rm ES} = \frac{\hbar E_0}{N}\left(\frac{2\pi}{\phi_0}\right)^2 \sum_{|j|=1}^{N/2}\left(\frac{1}{C_{\rm l}\omega_j}a_j^\dagger\hat{a}_j + \frac{1}{C_{\rm r}\upsilon_j}\hat{b}_j^\dagger\hat{b}_j\right), \tag{17}$$

which describes the shift of the bare energies and frequencies in both transmission lines. We can therefore redefine the noninteracting Hamiltonian by including this term as $\hat{\mathcal{H}}_0 = \hat{\mathcal{H}}_{\rm L} + \hat{\mathcal{H}}_{\rm R} + \hat{\mathcal{H}}_{\rm ES}$. The energy shift of the bare eigenenergies in the LHTL is simply given by

$$\tilde{\epsilon}_j = \epsilon_j + \frac{\hbar E_0}{NC_{\rm l}\omega_j}\left(\frac{2\pi}{\phi_0}\right)^2. \tag{18}$$

To see the frequency shift clearly, we now introduce the corrected dispersion relations of the LHTL and the RHTL as follows:

$$\tilde{\omega}_j = \omega_j + \frac{E_0}{4NC_{\rm l}\omega_j\sin^2\left(\frac{k_j\,\Delta x}{2}\right)}\left(\frac{2\pi}{\phi_0}\right)^2, \tag{19}$$

$$\tilde{\upsilon}_j = \upsilon_j + \frac{E_0}{NC_{\rm r}\upsilon_j}\left(\frac{2\pi}{\phi_0}\right)^2. \tag{20}$$

These are obtained by letting the ladder operators evolve in the interaction picture, and exploiting the commutation rules in Eqs. (10) and (11):

$$\hat{a}_j^{\rm I}(t) = \hat{U}_0^\dagger(t)\hat{a}_j\hat{U}_0(t) = \hat{a}_j e^{-i\tilde{\omega}_j t}, \tag{21}$$

$$\hat{b}_j^{\rm I}(t) = \hat{U}_0^\dagger(t)\hat{b}_j\hat{U}_0(t) = \hat{b}_j e^{-i\tilde{\upsilon}_j t}, \tag{22}$$

where $\hat{U}_0 = e^{-i\mathcal{H}_0 t/\hbar}$. Each corrected frequency consists of the sum of the bare frequency and a correcting term. Interestingly, in both LHTL and RHTL such correcting terms decrease monotonically with the wave vector.

Now we want to focus on the possibility to transmit excitations through the SQUID. We notice that the only element in the interaction Hamiltonian allowing the exchange of excitations between the two parts of the CTL is

$$\hat{\mathcal{H}}^{\rm I}_{\rm HP} = \sum_{i,j}^{N/2} g_{ij}\left(\hat{a}_i\hat{b}_j^\dagger e^{-i(\tilde{\omega}_i-\tilde{\upsilon}_j)t+i(k_i-p_j)\Delta x} + \text{h.c.}\right), \tag{23}$$

where we defined the coupling constants $g_{ij} = -\frac{\hbar E_0}{N\sqrt{C_{\rm l}C_{\rm r}\omega_i\upsilon_j}}\left(\frac{2\pi}{\phi_0}\right)^2$. This term describes the hopping effect between the two TLs, namely the annihilation of one excitation on one side of the CTL and the creation of another excitation on the other side. The hopping effect between two modes of the two TLs can be activated by imposing the frequency and momentum conservation of the two magnetic flux fields at the SQUID. However, as a consequence of the discreteness of the mode structure, the propagation of quantum excitations through the SQUID does not result possible for all mode pairs, but only for those modes of the magnetic flux fields fulfilling the phase matching conditions given by $k_i = p_j$ (momentum conservation) and the transcendental equation $\tilde{\omega}_i = \tilde{\upsilon}_j$ (frequency conservation). Since the momentum conservation of process is fulfilled by modes with the same mode number, the

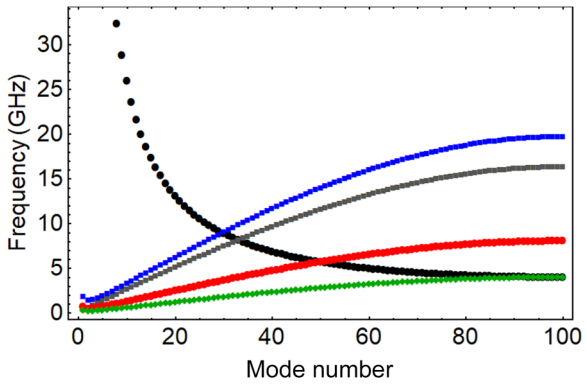

FIG. 2. Corrected dispersion relations $\tilde{\omega}_j$ (black) and bare eigenenergies $\tilde{\epsilon}_j/\hbar$ (gray) of the LHTL. Other colors label the corrected dispersion relations $\tilde{\upsilon}_j$ of the RHTL, calculated by solving the transcendental equation $\tilde{\omega}_j = \tilde{\upsilon}_j$, with j labeling the jth mode of both the LHTL and the RHTL, and using C_r as the variable. Frequencies of the RHTL are plotted ensuring the frequency matching for the mode pair $\tilde{\omega}_{30} = \tilde{\upsilon}_{30}$ (blue), $\tilde{\omega}_{50} = \tilde{\upsilon}_{50}$ (red), and $\tilde{\omega}_{100} = \tilde{\upsilon}_{100}$ (green), thereby obtaining $C_\mathrm{r} = 1.06$ pF, $C_\mathrm{r} = 6.19$ pF, and $C_\mathrm{r} = 24.71$ pF, respectively. Other parameters are as follows: $C_\mathrm{l} = 0.40$ pF, $L_\mathrm{r} = 0.25$ nH, $L_\mathrm{l} = 1.0$ nH, $I_\mathrm{c} = 1.25$ μA, and $N = 200$.

transcendental equation becomes $\tilde{\omega}_j = \tilde{\upsilon}_j$, and it is solved by tuning the set of parameters $\{C_\mathrm{l}, C_\mathrm{r}, L_\mathrm{l}, L_\mathrm{r}\}$ opportunely. The discrete mode structure of both TLs therefore allows the propagation of excitations to be restricted between the two TLs to only two selected modes, thereby limiting undesired hopping effects between the other modes.

To make a concrete example, in Fig. 2 we plot the LHTL eigenenergies in Fig. (18), as well as the dispersion relations in Eqs. (19) and (20). The two dispersion relations are obtained by selecting a set of parameters $\{C_\mathrm{l}, L_\mathrm{l}, L_\mathrm{r}\}$, and fixing a determined resonant mode pair by solving the trascendental equation $\tilde{\omega}_j = \tilde{\upsilon}_j$ with respect to the capacitance of the RHTL, C_r. We solved this equation for three set of modes, namely $\tilde{\omega}_{100} = \tilde{\upsilon}_{100}$, $\tilde{\omega}_{50} = \tilde{\upsilon}_{50}$, and $\tilde{\omega}_{30} = \tilde{\upsilon}_{30}$, obtaining three different values of C_r, then we plotted the dispersion relations.

IV. INTERACTION AND DYNAMICS

In the last section we observed that we can control the set of parameters $\{C_\mathrm{l}, C_\mathrm{r}, L_\mathrm{l}, L_\mathrm{r}\}$ to enable the propagation of quanta of the magnetic flux fields between two modes of the LHTL and the RHTL. All other terms in Eq. (23) describing the interaction between two off-resonant modes do not fulfill the phase-matching conditions, and their contribution is in fact negligible. This allows us to drastically reduce the Hilbert space of the system, thereby focusing on few modes of the CTL.

The possibility to isolate the contribution of specific mode pairs and ignore all secularities (i.e., off-resonant terms) can be applied to other interaction terms accounted in the Hamiltonian in Eq. (16). In particular, since we are interested in the interaction between the LHTL and the RHTL, we can tailor the set $\{\Omega, C_\mathrm{l}, C_\mathrm{r}, L_\mathrm{l}, L_\mathrm{r}\}$, thereby ensuring the phase matching for only one coupling term in Eq. (16) containing products of ladder operators stemming from different TLs. Note that the presence of the modulation frequency Ω is fundamental for the activation of Raman coupling or squeezing terms, which otherwise would be counter-rotating and therefore negligible after the rotating-wave approximation (RWA).

The possibility to control the Hamiltonian in Eq. (16) and activate one of the possible interaction terms according to our needs makes this device an interesting platform for the simulation of typical scenarios in quantum optics and quantum information. In what follows, we present some possible application of our findings. We stress that, although we might consider also the coupling between modes within the same TL, henceforth we will focus on the interaction of modes stemming from the LHTL and the RHTL. We will always assume that the two resonant modes are characterized by the same mode number j, thereby omitting the label j henceforth.

Note that this choice highlights one of the most impressive features of our CTL: the coupling strength ξ of two interacting modes with the same mode number does not depend on the mode number, but it is identical for any mode pair. This becomes more evident by looking at Eq. (14): once we expand the square in the curly brackets and look at cross interactions between modes with the same mode number j, we notice that each coupling parameter takes the form

$$\xi \propto \frac{E_0}{N\sqrt{C_\mathrm{r}C_\mathrm{l}}\omega_j \upsilon_j}\left(\frac{2\pi}{\phi_0}\right)^2 = \frac{E_0}{N}\left(\frac{L_\mathrm{r}L_\mathrm{l}}{C_\mathrm{r}C_\mathrm{l}}\right)^{\frac{1}{4}}\left(\frac{2\pi}{\phi_0}\right)^2. \tag{24}$$

We note that the product between mode frequencies of the CTL characterized by the same label j does not depend on the mode number, $\omega_j \upsilon_j = 1/\sqrt{C_\mathrm{r}C_\mathrm{l}L_\mathrm{r}L_\mathrm{l}}$, see Eqs. (7) and (8). This peculiar feature of the CTL stems straightforwardly from the fact that we are joining a LHTL and a RHTL, and cannot be observed in platforms based on only left-handed or right-handed transmission lines. Remarkable implications of this feature are discussed in Sec. VI D.

A. Excitation hopping

As a first scenario, we again consider the interaction

$$\hat{\mathcal{H}}_\mathrm{I} = \hbar\xi_\mathrm{hp}\left(\hat{a}^\dagger\hat{b} + \hat{a}\hat{b}^\dagger\right), \tag{25}$$

with coupling constant

$$\xi_{\mathrm{hp}} = -\frac{2E_0}{N}\left(\frac{L_{\mathrm{r}}L_{\mathrm{l}}}{C_{\mathrm{r}}C_{\mathrm{l}}}\right)^{\frac{1}{4}}\left(\frac{2\pi}{\phi_0}\right)^2. \tag{26}$$

This Hamiltonian can be calculated from Eq. (23) by tailoring the parameters such that $\tilde{\omega} = \tilde{\upsilon}$ and performing the RWA. Note that to accomplish this result we did not require the modulation of the Josephson energy at the SQUID. In the Heisenberg picture, the annihilation operators for the two TLs evolve as follows:

$$\hat{a}(t) = e^{-i\omega t}\left(\hat{a}\cos(\xi_{\mathrm{hp}}t) + i\hat{b}\sin(\xi_{\mathrm{hp}}t)\right), \tag{27a}$$

$$\hat{b}(t) = e^{-i\omega t}\left(\hat{b}\cos(\xi_{\mathrm{hp}}t) + i\hat{a}\sin(\xi_{\mathrm{hp}}t)\right). \tag{27b}$$

This Hamiltonian describes a collinear beam splitting, in which the transmission and reflection parameters are modulated in time by the coupling constant ξ_{hp}. This type of interaction therefore expresses the propagation of excitations along the CTL due to the annihilation of one excitation on one of the two TLs and the creation of one excitation with same frequency and momentum on the other one.

B. Raman scattering

A second interesting scenario is delineated by the Hamiltonian

$$\hat{\mathcal{H}}_{\mathrm{I}} = \hbar\xi_{\mathrm{rm}}\left(\hat{a}^\dagger\hat{b} + \hat{a}\hat{b}^\dagger\right), \tag{28}$$

which is structurally identical to Eq. (25) but with coupling constant

$$\xi_{\mathrm{rm}} = -\frac{\eta E_0}{N}\left(\frac{L_{\mathrm{r}}L_{\mathrm{l}}}{C_{\mathrm{r}}C_{\mathrm{l}}}\right)^{\frac{1}{4}}\left(\frac{2\pi}{\phi_0}\right)^2. \tag{29}$$

To obtain this Hamiltonian, we tune the SQUID modulation frequency such that $\tilde{\omega} = \tilde{\upsilon} + \Omega$, assuming that $\tilde{\omega} > \tilde{\upsilon}$. In contrast to the previous case, the frequencies of the two interacting modes differ, and the frequency conservation is only guaranteed by the modulation of the Josephson energy at the SQUID. This interaction gives rise to two possible phenomena: the Stokes Raman scattering, when the SQUID induces the decay of a LHE into a lower-energetic RHE; the anti-Stokes Raman scattering, when the SQUID pumps the mode $\tilde{\upsilon}$ of the RHTL, which decays into a LHE $\tilde{\omega}$ with higher energy. Clearly, we can manipulate our parameters thereby activating a resonance of the form $\tilde{\upsilon} = \tilde{\omega} + \Omega$, with $\tilde{\upsilon} > \tilde{\omega}$.

One of the remarkable facts stemming from combining two TLs with different dispersion relations is that the Raman effect can also occur between modes of the two TLs having the same bare energy $\tilde{\epsilon} = \hbar\tilde{\upsilon}$. After the Raman scattering in the SQUID, a signal generated in the RHTL would therefore propagate to the LHTL with amplified frequency but the same wave vector and bare energy [67].

As before, we report the annihilation operators of the two modes $\tilde{\omega}$ and $\tilde{\upsilon}$ evolved in the Heisenberg picture:

$$\hat{a}(t) = e^{-i\tilde{\omega}t}\left(\hat{a}\cos(\xi_{\mathrm{rm}}t) + i\hat{b}\sin(\xi_{\mathrm{rm}}t)\right), \tag{30a}$$

$$\hat{b}(t) = e^{-i\tilde{\upsilon}t}\left(\hat{b}\cos(\xi_{\mathrm{rm}}t) + i\hat{a}\sin(\xi_{\mathrm{rm}}t)\right). \tag{30b}$$

Despite the evident similarities between the annihilation operators written above and those in Eq. (27), we stress that this interaction mixes two input modes with different frequencies.

C. Two-mode squeezing

The modulation of the SQUID can give rise to another interesting scenario. Indeed, by activating the resonance condition $\Omega = \tilde{\omega} + \tilde{\upsilon}$ we can squeeze the state of two modes stemming from two different TLs. Once we fix the resonance condition written above, ensure the momentum conservation $p = -k$, and apply the RWA, the Hamiltonian describing the two-mode squeezing coupling reads

$$\hat{\mathcal{H}}_{\mathrm{I}} = \hbar\xi_{\mathrm{sq}}\left(\hat{a}^\dagger\hat{b}^\dagger + \hat{a}\hat{b}\right), \tag{31}$$

and the annihilation operators in the Heisenberg picture evolve as

$$\hat{a}(t) = e^{-i\tilde{\omega}t}\left(\hat{a}\cosh(\xi_{\mathrm{sq}}t) - i\hat{b}^\dagger\sinh(\xi_{\mathrm{sq}}t)\right), \tag{32a}$$

$$\hat{b}(t) = e^{-i\tilde{\upsilon}t}\left(\hat{b}\cosh(\xi_{\mathrm{sq}}t) - i\hat{a}^\dagger\sinh(\xi_{\mathrm{sq}}t)\right), \tag{32b}$$

with squeezing parameter ξ_{sq} equal to ξ_{rm} in Eq. (29). These operators suggest to us that we can squeeze the quantum vacuum of the two transmission lines at the same time, thereby generating one LHE and one RHE. Phenomena of this kind play a crucial role in nonlinear optics. An example is the parametric down-conversion, in which a pump laser interacts with a nonlinear material generating two entangled and spatially distinguishable photons, named signal and idler photons [68–71].

Before concluding this section, we need to stress that the three types of interaction presented so far, namely the hopping effect, the Raman effect and the two-mode squeezing, differ in intensity. This is due to the fact that the coupling constant ξ_{sq} (or ξ_{rm}) mainly differs from ξ_{hp} by a factor η. In order for our mathematical description of the CTL to be consistent, we needed to assume a regime of small oscillation, $\eta \ll 1$. A reasonable value for the dimensionless oscillation amplitude is $\eta = 0.1$, although higher values have been considered in the same regime [39,40].

V. CORRELATIONS BETWEEN THE TLS

In this section we study the correlations between two modes of the LHTL and the RHTL interacting resonantly. Our approach is based on the second-order correlation function, which, for our purpose, assumes the following expression [72]:

$$G^{(2)}(n_\mathrm{l},t_1;n_\mathrm{r},t_2)=\langle\Phi^{\mathrm{L}(-)}(n_\mathrm{l},t_1)\Phi^{\mathrm{R}(-)}(n_\mathrm{r},t_2)\Phi^{\mathrm{L}(+)}(n_\mathrm{l},t_1)\Phi^{\mathrm{R}(+)}(n_\mathrm{r},t_2)\rangle. \tag{33}$$

Sometimes we will make use of the normalized second-order correlation function,

$$g^{(2)}(n_\mathrm{l},t_1;n_\mathrm{r},t_2)=\frac{G^{(2)}(n_\mathrm{l},t_1;n_\mathrm{r},t_2)}{G^{(1)}(n_\mathrm{l},t_1)G^{(1)}(n_\mathrm{r},t_2)}, \tag{34}$$

where $G^{(1)}(n,t)=\langle\Phi^{(-)}(n,t)\Phi^{(+)}(n,t)\rangle$ is the first-order correlation function.

We initialize the system in the two-mode Fock state $|\psi(0)\rangle=|s_\mathrm{L},s_\mathrm{R}\rangle$, where s_L and s_R represent the number of excitations of the modes with frequencies $\tilde{\omega}$ and $\tilde{\upsilon}$, respectively. This reduces the correlation function to

$$G^{(2)}_{s_\mathrm{L},s_\mathrm{R}}(t_1,t_2)=\sqrt{\frac{L_\mathrm{r}L_\mathrm{l}}{C_\mathrm{r}C_\mathrm{l}}}\frac{\hbar^2}{N^2}\langle\hat{a}^\dagger(t_1)\hat{b}^\dagger(t_2)\hat{a}(t_1)\hat{b}(t_2)\rangle. \tag{35}$$

The explicit form of the correlation function depends on the specific resonance we are interested in. In what follows, we will analyze the three cases studied before, namely the excitation hopping, the Raman scattering, and the two-mode squeezing. Note that, despite the different physical interpretation of the two scenarios in Secs. IV A and IV B, the annihilation (and therefore also the creation) operators in Eqs. (27) and (30) lead to the same form of the correlation function, therefore these two cases will be presented together.

A. Excitation hopping and Raman scattering

We now fix the parameters of the CTL such that the energy conservation is fulfilled either in terms of $\tilde{\omega}=\tilde{\upsilon}$, or $\tilde{\omega}=\tilde{\upsilon}+\Omega$. As mentioned above, the second-order correlation function is structurally identical for the two scenarios, and reads

$$G^{(2)}_{s_h,s_d}(t_1,t_2)=\sqrt{\frac{L_\mathrm{r}L_\mathrm{l}}{C_\mathrm{r}C_\mathrm{l}}}\frac{\hbar^2 s_\mathrm{L}s_\mathrm{R}C_1^2C_2^2}{N^2}\times\left[(1-T_1T_2)^2+\frac{s_\mathrm{L}-1}{s_\mathrm{R}}T_2^2+\frac{s_\mathrm{R}-1}{s_\mathrm{L}}T_1^2\right], \tag{36}$$

where we defined $C_j=\cos(\xi t_j)$ and $T_j=\tan(\xi t_j)$, with $|j|=1,2$. Here, ξ corresponds to either ξ_hp or ξ_rm. Clearly, when the CTL is prepared in the vacuum state, or when only one excitation populates the CTL, the correlation function is identically zero. However, it is particularly interesting to consider the case when the CTL is initially populated by two excitations, each stemming from a different TL. In this case, the normalized second-order correlation function becomes

$$g^{(2)}_{1_\mathrm{L},1_\mathrm{R}}(t_1,t_2)=\cos^2[\xi(t_1+t_2)]. \tag{37}$$

This correlation function tells us that the coincidence probability to detect two particles at different TLs is modulated, and that periodically this probability reaches zero. To see what happens to the two particles when $g^{(2)}_{1_\mathrm{L},1_\mathrm{R}}(t_1,t_2)=0$, we let the system evolve in the Schrödinger picture. Since the initial state consists of two excitations in different channels, this is equivalent to applying the creation operators $\hat{a}^\dagger(t)$ and $\hat{b}^\dagger(t)$ in Eq. (27) or Eq. (30) to the vacuum state, $|\psi(t)\rangle=\hat{a}^\dagger(t)\hat{b}^\dagger(t)|0_\mathrm{L},0_\mathrm{R}\rangle$, hence obtaining

$$|\psi(t)\rangle=e^{i(\tilde{\omega}+\tilde{\upsilon})t}\cos(2\xi\,t)\,|1_\mathrm{L},1_\mathrm{R}\rangle+i\,e^{i(\tilde{\omega}+\tilde{\upsilon})t}\sin(2\xi\,t)\,(|0_\mathrm{L},2_\mathrm{R}\rangle+|2_\mathrm{L},0_\mathrm{R}\rangle). \tag{38}$$

As we can see, the normalized correlation function in Eq. (37) with $t_1=t_2=t$ corresponds to the square of the first term of the output state, which describes the probability to detect two excitations in two different modes. When this probability vanishes at time $t_\mathrm{dip}=\pi/(4\xi)$, the probability to find two excitations at the same TL is maximized. The state $|\psi(t_\mathrm{dip})\rangle$ therefore corresponds to the output state of a quantum interference scenario, in which two particles interacting in a beam splitter are only found both in one of the two output channels. In quantum optics, the phenomenon in which the quantum interference of two particles annuls the coincidence probability and generates the two-photon NOON state, is referred to as the Hong-Ou-Mandel effect, and it finds applications in many quantum optical frameworks [73–76].

B. Two-mode squeezing

To conclude this section, we analyze the second-order correlation function when the resonance $\Omega=\tilde{\omega}+\tilde{\upsilon}$ is activated. Substituting Eq. (32) into Eq. (35) we obtain

$$G^{(2)}_{s_h,s_d}(t_1,t_2)=\sqrt{\frac{L_rL_l}{C_rC_l}}\frac{\hbar^2 s_L s_R \bar{C}_1^2\bar{C}_2^2}{N^2}\left[1+\bar{T}_1\bar{T}_2+\frac{(s_L+1)(s_R+1)}{s_L s_R}(\bar{T}_1^2\bar{T}_2^2+\bar{T}_1\bar{T}_2)+\frac{s_L+1}{s_R}\bar{T}_2^2+\frac{s_R+1}{s_L}\bar{T}_1^2\right], \quad (39)$$

where we defined $\bar{C}_j=\cosh(\xi_{sq}t_j)$ and $\bar{T}_j=\tanh(\xi_{sq}t_j)$, with $|j|=1,2$. This function describes the correlations between the LHTL and the RHTL when the two modes of interest are prepared in a Fock state with s_L and s_R excitations, respectively.

We notice that in the limit $t_1=t_2\gg 1/\xi_{sq}$, we have $\bar{T}_1=\bar{T}_2\simeq 1$ and the normalized correlation function does not depend on time,

$$g^{(2)}_{s_L,s_R}=1+\frac{1}{s_L+s_R+1}+\frac{2s_Rs_L}{(s_L+s_R+1)^2}. \quad (40)$$

This function has been predicted in Ref. [77]. Interestingly, it only depends on the initial number of excitations, and is bounded in the range $1<g^{(2)}_{s_L,s_R}\leq 2$. As expected for two-mode squeezed states, the second-order correlation function does not vanish when the system is prepared in the vacuum state, $s_L=s_R=0$. Indeed in this case the normalized second-order correlation function asymptotically approaches to $g^{(2)}_{0_L,0_R}=2$, and the two modes individually show the statistics of a thermal state.

To consider a further case of interest beyond the vacuum state, we assume that only one of the two TLs, say the LHTL, is populated, whereas the other one is prepared in the vacuum state, $s_L=s$ and $s_R=0$. In this scenario, the normalized second-order correlation function reduces to

$$g^{(2)}_{s,0}=1+\frac{1}{s+1}. \quad (41)$$

Interestingly, this function tends to $g^{(2)}_{s,0}\simeq 1$ for highly populated Fock states, $s\gg 1$. Note that the normalized correlation function, which determines the first-order coherence between the LHTL and the RHTL, defined as

$$g^{(1)}(n_l,t_l;n_r,t_2)=\frac{G^{(1)}(n_l,t_l;n_r,t_2)}{\sqrt{G^{(1)}(n_l,t_l)G^{(1)}(n_r,t_2)}}, \quad (42)$$

with $G^{(1)}(n_l,t_l;n_r,t_2)=\langle\Phi^{L(-)}(n_l,t_l)\Phi^{R(-)}(n_r,t_2)\rangle$, is identically zero in the presence of two-mode squeezing. Therefore, the system shows second-order coherence but not first-order coherence.

VI. FURTHER QUANTUM SIMULATION SCENARIOS

So far we have presented our platform as possible quantum simulator of standard phenomena in quantum optics. However, the versatility of this device suggests further possible uses in other branches of physics, such as in quantum mechanics, multimode quantum systems, and quantum thermodynamics. In what follows, we will briefly discuss these three cases.

A. General two-mode coupling for degenerate QHOs

In quantum mechanics, the Hamiltonian of two interacting bosonic modes induces a linear dynamics when all annihilation and creation operators appear as combinations of quadratic terms [78]. These types of Hamiltonian are largely employed in quantum optics, and in this work we already discussed three scenarios of interest. In Sec. IV A, for example, we discussed a beam-splitting interaction, in which the Hamiltonian in Eq. (25) stems from the resonant activation of hopping terms. On the other hand, in Sec. IV C the Hamiltonian in Eq. (31) only contains the two-mode squeezing terms. In both cases, we made use of the RWA to get rid of highly oscillating terms that do not fulfil the energy conservation. However, the resonance conditions enabling the filtering of the hopping terms and the squeezing terms from Eq. (16) do not exclude themselves reciprocally, but they can be activated together by properly tuning the modulation of the Josephson energy. Once we assume $\tilde{\omega}=\tilde{\upsilon}=\omega$ and $\Omega=2\omega$, the interaction Hamiltonian becomes

$$\hat{\mathcal{H}}_I=\hbar\xi_{hp}\left(\hat{a}^\dagger\hat{b}+\hat{a}\hat{b}^\dagger\right)+\hbar\xi_{sq}\left(\hat{a}^\dagger\hat{b}^\dagger+\hat{a}\hat{b}\right)+\hbar\xi_{sl}\left[(\hat{a}^\dagger)^2+\hat{a}^2\right]+\hbar\xi_{sr}\left[(\hat{b}^\dagger)^2+\hat{b}^2\right], \quad (43)$$

where in the second line we introduced the single-mode squeezing coupling terms, weighed by the squeezing parameters for the LHTL and the RHTL mode,

$$\xi_{sl}=-\frac{\eta E_0}{NC_l\omega}\left(\frac{2\pi}{\phi_0}\right)^2, \quad (44)$$

$$\xi_{sr}=-\frac{\eta E_0}{NC_r\upsilon}\left(\frac{2\pi}{\phi_0}\right)^2, \quad (45)$$

respectively. This Hamiltonian describes the most general linear interaction between two distinguishable quantum harmonic oscillators (QHOs) characterized by the same frequency. The dynamics stemming from Eq. (43) was largely studied by means of the symplectic formalism in Ref. [78].

B. Multimode quantum system interaction

In this section we want to discuss the possibility to extend our model to a larger set of interacting bosonic

degrees of freedom. We can realize this scenario by shaping the modulation of the Josephson energy as the superposition of M periodic functions:

$$E(t) = E_0 \left[1 + \sum_{m=1}^{M} (\eta_m \sin(\Omega_m t) + \kappa_m \cos(\Omega_m t)) \right], \quad (46)$$

with η_m and κ_m oscillation amplitudes, and Ω_m being the frequency of the mth periodic function.

By choosing the frequencies Ω_m opportunely, we can therefore activate further resonances and select further interacting modes. This allows us, on the one hand, to extend the scenarios analyzed so far (beam-splitting interactions, Raman scatterings, two-mode squeezing interactions) to a larger number of interacting mode pairs; on the other hand, we can prepare an exotic Hamiltonian describing multimode interactions.

As a first example, we can prepare two distinguishable and nondegenerate interacting QHOs [79]. To do this, we tailor the Josephson energy of the SQUID in Eq. (46) (with $M = 2$) by imposing $\Omega_1 = \tilde{\omega}_h - \tilde{\upsilon}$, $\Omega_2 = \tilde{\omega}_h + \tilde{\upsilon}$, $\eta_1 = \eta_2 = 0$, and $\kappa_1 = \kappa_2 = 2$. Once we set the parameters as above, the interaction Hamiltonian reduces to

$$\hat{\mathcal{H}}_{\rm I} = \hbar\xi \left(\hat{a} + \hat{a}^\dagger\right)\left(\hat{b} + \hat{b}^\dagger\right), \quad (47)$$

where $\xi = \xi_{\rm rm}$ in Eq. (29). The eigenmodes deriving from the diagonalization of this Hamiltonian are sometimes referred to as polaritons [80], and their dynamics is well known in the literature [78].

Interestingly, the possibility to activate more resonances by means of the modulation of the Josephson energy in Eq. (46) permits a drastic extension of the number of interacting modes, and consequently of the Hilbert space. As an example, we can prepare the general Hamiltonian of a three-mode system:

$$\hat{\mathcal{H}}_{\rm I} = \hbar\Big[\xi_1 \left(\hat{c}_i + \hat{c}_i^\dagger\right)\left(\hat{c}_j + \hat{c}_j^\dagger\right) + \xi_2 \left(\hat{c}_i + \hat{c}_i^\dagger\right)\left(\hat{c}_k + \hat{c}_k^\dagger\right) + \xi_3 \left(\hat{c}_j + \hat{c}_j^\dagger\right)\left(\hat{c}_k + \hat{c}_k^\dagger\right)\Big], \quad (48)$$

with ξ_1, ξ_2, and ξ_3 coupling constants, and with $c = a, b$ representing one mode of either the LHTL or the RHTL. This Hamiltonian describes three selected modes of the CTL, each thereof is interacting with the other one.

C. CTL as the quantum thermal machine

Finally, we want to discuss some interesting applications of our system in quantum thermodynamics. The idea is to employ the CTL as a quantum thermal machine [81,82], which can either convert heat into work (quantum heat engine) [83,84] or cool down a cold bath (quantum refrigerator) [83,85]. A model of quantum heat engine is the quantum amplifier, in which two bosonic modes, coupled to two baths at different temperatures, interact by means of an external drive to generate output power [83]. To let our device work as a quantum amplifier, we need to thermalize two modes of the CTL, say $\tilde{\omega}$ and $\tilde{\upsilon}$, by coupling them to two baths at different temperatures: assuming $\tilde{\omega} > \tilde{\upsilon}$, the LHTL mode is coupled to a hot bath at temperature $T_{\rm h}$, whereas the RHTL is coupled to a cold bath at temperature $T_{\rm c}$. The required resonance condition we need to exploit is the Raman scattering $\Omega = \tilde{\omega} - \tilde{\upsilon}$. The interaction Hamiltonian written in the Schrödinger picture is

$$\hat{\mathcal{H}}_{\rm I}(t) = \hbar\xi \left(e^{i\Omega t}\hat{a}\hat{b}^\dagger + e^{-i\Omega t}\hat{a}^\dagger\hat{b}\right), \quad (49)$$

where we again assumed a modulation of the Josephson energy of the form $E(t) = E_0(1 + \eta\cos(\Omega t))$. By carrying out the time derivative of this Hamiltonian and averaging it with respect to the state, we get the amplifier output power [83]:

$$\mathcal{P}(t) = i\hbar\Omega\xi \left(e^{i\Omega t}\langle\hat{a}\hat{b}^\dagger\rangle - e^{-i\Omega t}\langle\hat{a}^\dagger\hat{b}\rangle\right). \quad (50)$$

Another powerful application of our CTL is the realization of a quantum network [60,86]. In the context of

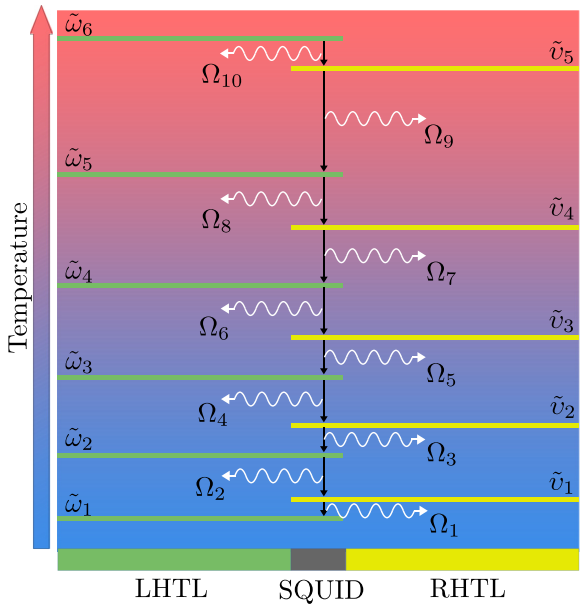

FIG. 3. Schematic representation of the cascade quantum network. The modulation frequencies Ω_m of the Josephson energy are set thereby activating the Raman resonances between modes of the LHTL and the RHTL. Every resonant mode of the CTL is coupled to a bath at temperature T_{n_x}, with $x = l, r$. Higher frequency modes of the CTL are coupled to baths with higher temperatures. Therefore, the SQUID extracts work at each step of the Raman cascade. The subscripts on the frequencies simply differentiate the mode frequencies and do not refer to any specific modes.

quantum thermodynamics, a quantum network consists of an ensemble of wires and junctions, which allows the heat propagation and the extraction of net work. The multimode structure of the CTL, along with the possibility to activate multiple resonances (as shown in the previous section), suggest that the CTL itself can act as a quantum network. A model of the quantum network can be realized by coupling the modes of the LHTL and the RHTL to different baths and activating chains of Raman resonances by means of a tailored modulation of the Josephson energy. The cascade quantum amplifier is pictorially represented in Fig. 3. The higher the mode frequency, the higher the temperature of the bath the mode is coupled with. The chain of Raman resonances activates the heat flow from the higher temperature baths towards the cooler temperature ones, whereas the SQUID extracts power at each Raman decay. More details about the implementation of this quantum heat engine on our CTL platform, as well as the analysis of the heat flows and the extracted power, are left for a future publication.

D. Maximal entanglement of multimode bipartite systems

The employment of the transmission line depicted in Fig. 1 enables the simulation of scenarios, which are unfeasible in common quantum optical platforms. To make a concrete example, we discuss the possibility to create maximally entangled bipartite states. Let us assume that the modulation of the Josephson energy at the SQUID can be decomposed in terms of M harmonic oscillations,

$$E(t) = E_0 \left[1 + \eta \sum_{j=1}^{M} \cos(\Omega_j t) \right], \tag{51}$$

where each frequency Ω_j fulfills the squeezing resonance condition discussed in Sec. IV C for the two modes with frequencies ω_j and υ_j, namely $\Omega_j = \tilde{\omega}_j + \tilde{\upsilon}_j$. Once we move to the interaction picture and carry out the RWA, the total Hilbert space of the interacting modes reduces to the tensor product between the M-dimensional Hilbert subspace of the LHTL and the M-dimensional Hilbert subspace of the RHTL. The noninteracting Hamiltonian therefore reads

$$\hat{\mathcal{H}}_0 = \hbar \sum_{j=1}^{M} \left[4\omega_j \sin^2\left(\frac{k_j \Delta x}{2}\right) \hat{a}_j^\dagger \hat{a}_j + \upsilon_j \hat{b}_j^\dagger \hat{b}_j \right]. \tag{52}$$

In this scenario, the interaction Hamiltonian becomes

$$\hat{\mathcal{H}}_{\rm I} = \hat{\mathcal{H}}_{\rm ES} + \hat{\mathcal{H}}_{\rm 2S}, \tag{53}$$

where the first term describes the usual frequency shift, see Eq. (17), whereas the second term is

$$\hat{\mathcal{H}}_{\rm 2S} = \hbar \xi_{\rm sq} \sum_{j=1}^{M} \left(\hat{a}_j \hat{b}_j + \hat{a}_j^\dagger \hat{b}_j^\dagger \right), \tag{54}$$

and it is responsible for the two-mode squeezing of each mode pair labeled by i. Of note, the coupling constant

$$\xi_{\rm sq} = -\frac{\eta E_0}{N\sqrt{C_{\rm r} C_{\rm l} \omega_j \upsilon_j}} \left(\frac{2\pi}{\phi_0}\right)^2 = -\frac{\eta E_0 \, (L_{\rm r} L_{\rm l})^{\frac{1}{4}}}{N (C_{\rm r} C_{\rm l})^{\frac{1}{4}}} \left(\frac{2\pi}{\phi_0}\right)^2 \tag{55}$$

is not labeled by j. This is a direct consequence of the dispersion relations in Eqs. (7) and (8), whose product does not depend on the mode number as long as we couple two modes of the CTL with the same wave vector.

We now evolve the state of the CTL in the interaction picture by means of the unitary operator

$$\hat{U}_{\rm I}(t) = e^{-i\hat{\mathcal{H}}_{\rm 2S} t/\hbar} = \bigotimes_{j=1}^{M} e^{-i\xi_{\rm sq} t \left(\hat{a}_j \hat{b}_j + \hat{a}_j^\dagger \hat{b}_j^\dagger\right)}. \tag{56}$$

We recall that the energy shift due to the Hamiltonian $\hat{\mathcal{H}}_{\rm ES}$ has been incorporated in $\hat{\mathcal{H}}_0$. The unitary operator in Eq. (56) can be interpreted as the product of two-mode squeezing operators, each acting on two modes of the CTL with the same wave vector. In the low-gain regime $\eta \ll 1$, if the CTL was initially prepared in the vacuum state $|{\rm vac}\rangle$, the final state at time $t = t_{\rm f}$ corresponds to

$$\begin{aligned} |\psi(t_{\rm f})\rangle = \hat{U}_{\rm I}(t_{\rm f})|{\rm vac}\rangle &\simeq \left(\hat{\mathbb{1}} - \xi_{\rm sq} t_{\rm f} \sum_{j=1}^{M} \hat{a}_j^\dagger \hat{b}_j^\dagger \right) |{\rm vac}\rangle \\ &\simeq |{\rm vac}\rangle + g \sum_{j=1}^{M} |{\rm L}_j\rangle |{\rm R}_j\rangle, \end{aligned} \tag{57}$$

where in the second line we both introduced the probability amplitude $g = -\xi_{\rm sq} t_{\rm f}$ and relabeled the quantum state of system in terms of products of the form $|{\rm L}_l\rangle|{\rm R}_m\rangle$ to indicate the presence of one photon in the LTHL with mode number l, and one photon in the RHTL with mode number m.

If we ignore the contribution of the vacuum state, we observe that the final state is already expressed in the basis of the Schmidt modes [87–89]. This allows us to quantify the degree of entanglement by means of the Schmidt number. In the low-gain regime, given a state expressed in the basis of the Schmidt modes $|\psi\rangle = \sum_j c_j |{\rm L}_j\rangle|{\rm R}_j\rangle$, the Schmidt number is defined as $K = 1/\sum_j |c_j|^4$ [87,89]. In our case, once we normalize the final state it becomes clear that each term of the sum contributes with equal probability $|c_j|^2 = 1/M$, therefore the Schmidt number is equal to

the dimension of Hilbert space of each subsystem, $K = M$, and the quantum state is maximally entangled.

We stress that we could obtain the maximal entangled state thanks to the fact that, once we set the coupling between mode pairs characterized by the same mode number, the coupling constant ξ_{sq} does not depend on the mode number but it only depends on circuit parameters. In quantum optics, one of the standard strategies for the generation of bipartite multimode entangled state consists of the use of the parametric down-conversion [90–93]. However, despite the possibility to entangle a large number of modes, the coupling between each mode pair always depends on the mode number, and the state can never be maximally entangled. In contrast, thanks to the combination of two transmission lines with left-handed and right-handed dispersion relations we generate maximally entangled state by coupling nonlocal mode pairs of the CTL with the same mode number.

E. High nonlinearity: quartic order interactions

When we have introduced our mathematical formalism in Sec. II, we have assumed that the amplitude of the magnetic flux at the SQUID is much smaller than the magnetic flux quantum in order to obtain the quadratic Lagrangian in the field amplitudes, Eq. (3). However, in the same regime we could also account for further perturbative effects stemming from high-order nonlinear interactions. To include such effects in the Hamiltonian, we require the expansion of the cosine function in Eq. (2c) up to the quartic power. By means of the same procedure as in Appendix A, we therefore obtain the following interaction Hamiltonian:

$$\mathcal{H}_{\rm I} \simeq \frac{E(t)}{2}\left(\frac{2\pi}{\phi_0}\right)^2 \left(\Phi_1^{\rm L} - \Phi_1^{\rm R}\right)^2 - \frac{E(t)}{24}\left(\frac{2\pi}{\phi_0}\right)^4 \left(\Phi_1^{\rm L} - \Phi_1^{\rm R}\right)^4 . \tag{58}$$

This classical Hamiltonian is quantized by means of the standard quantization protocol described in Appendix A.

The second line of the extended Hamiltonian given in Eq. (58) encompasses a large spectrum of highly nonlinear phenomena, which may not be easy to observe in a standard quantum optical apparatus. For the sake of simplicity, we focus our attention on the interaction between two modes of the two transmission lines. We stress that our CTL can isolate the coupling between two nonlocal modes without requiring any modulation of the Josephson energy at the SQUID. We simply need a set of parameters, which enables the two phase-matching conditions discussed in Sec. III to be fulfilled, namely the frequency and momentum conservation.

The Hamiltonian encoding the resonant interactions of two interacting modes reads [94]

$$\hat{\mathcal{H}}_{\rm I} = \hat{\mathcal{H}}_{\rm KE} + \hat{\mathcal{H}}_{\rm CK} + \hat{\mathcal{H}}_{\rm TPH} + \hat{\mathcal{H}}_{\rm KH} + \hat{\mathcal{H}}_{\rm KSQ} + \hat{\mathcal{H}}_{\rm DPC}. \tag{59}$$

The first two terms of this Hamiltonian, namely,

$$\hat{\mathcal{H}}_{\rm KE} = \xi_{{\rm K}_a}\left(\hat{a}^\dagger\hat{a}\right)^2 + \xi_{{\rm K}_b}\left(\hat{b}^\dagger\hat{b}\right)^2 \tag{60}$$

and

$$\hat{\mathcal{H}}_{\rm CK} = \xi_{\rm CK}\hat{a}^\dagger\hat{a}\,\hat{b}^\dagger\hat{b}, \tag{61}$$

correspond to two nonlinear Kerr frequency shifts. In particular, the former describes a self-Kerr effect due to the self-interaction of the two modes, whereas the latter describes the cross-Kerr interaction. Note that, in a regime where quartic interactions may be experimentally measurable [62,95], the theoretical model should always account for these terms, since they never oscillate in the interaction picture.

The two terms

$$\hat{\mathcal{H}}_{\rm KHP} = \xi_{\rm KHP}\hat{a}^\dagger\hat{a}(\hat{b}\,\hat{a}^\dagger + \hat{b}^\dagger\hat{a}) \tag{62}$$

and

$$\hat{\mathcal{H}}_{\rm THP} = \xi_{\rm THP}\left[\hat{a}^2(\hat{b}^\dagger)^2 + \hat{b}^2(\hat{a}^\dagger)^2\right] \tag{63}$$

describe two hopping effects. However, whereas the former describes a Kerr shift mediated by the hopping between two modes, the latter corresponds to the two-particle hopping, namely the propagation of excitation pairs between the two transmission lines. We notice that the two-photon hopping effect has been predicted in optomechanical systems [96]. The possibility to discriminate two spatially separated modes without necessarily tuning the Josephson energy of the SQUID makes this transmission line a perfect candidate to experimentally test this effect nonlocally in circuit QED.

Phenomena presented so far did not require any time dependence of the Josephson energy at the SQUID. Yet, the modulation of the Josephson energy as discussed in Sec. II would allow us to explore further scenarios. First, we mention that the two hopping effects introduced in Eqs. (62) and (63) would describe a frequency shift mediated by the Raman effect and the two-photon Raman effect if the modulation frequency of the Josephson energy fulfilled the resonant conditions $\Omega = \tilde{\omega} - \tilde{\upsilon}$ and $\Omega = 2\tilde{\omega} - 2\tilde{\upsilon}$, respectively. The other two relevant phenomena of interest emerging once we set proper resonant conditions are

encoded in the Hamiltonian operators

$$\hat{\mathcal{H}}_{\mathrm{KS}} = \xi_{\mathrm{KS}_a}\hat{a}^\dagger\hat{a}\left[\hat{b}^2 + \left(\hat{b}^\dagger\right)^2\right] + \xi_{\mathrm{KS}_b}\hat{b}^\dagger\hat{b}\left[\hat{a}^2 + \left(\hat{a}^\dagger\right)^2\right] \tag{64}$$

and

$$\hat{\mathcal{H}}_{\mathrm{DPC}} = \xi_{\mathrm{DPC}}\left[\hat{a}^2\hat{b}^2 + (\hat{a}^\dagger)^2(\hat{b}^\dagger)^2\right]. \tag{65}$$

The former describes the frequency shift of one mode caused by the squeezing of the other mode and it becomes relevant once we set the resonance condition $\Omega = 2\omega$ (or $\Omega = 2\upsilon$ if the two modes have different frequencies). The latter encodes the possibility to generate (annihilate) an excitation pair in the LTHL and an excitation pair in the RHTL. To activate this effect, we would need to impose the resonant condition $\Omega = 2\tilde{\omega} + 2\tilde{\upsilon}$.

Before concluding this section, we recall that tailored modulations of the Josephson energy could enable the activation of resonance conditions involving up to four different modes at the same time. Interestingly, as long as we couple mode pairs characterized by the same mode number, the interaction strength of each of these coupling terms in the Hamiltonian would not depend on the mode number. This can have relevant consequences in the engineering of highly entangled states in multipartite systems, as demonstrated in the previous section. Implications of multipartite interactions in our CTL are left for a future work.

VII. SUMMARY AND CONCLUSION

We have presented a hybrid platform realized by connecting a left-handed and a right-handed transmission line by means of a superconducting quantum interference device. After quantizing the magnetic flux fields in both TLs, we have investigated the phase matching at the SQUID, showing that the propagation of quantum excitations from one TL to the other one can occur only for two degenerate modes of the CTL.

We observed that the interaction between the two TLs occurs only between two modes fulfilling specific resonance conditions. We have shown that we can select the interacting modes, as well as the type of interaction, by controlling the set of circuit parameters. Among all possible interactions we could have activated, we have presented the hopping effect, the Raman scattering, and the two-mode squeezing. Considered more relevant for our discussion, we have focused our attention only on interactions between LHTL and RHTL modes.

As a result of our analysis, we have shown that our hybrid transmission line can simulate standard processes in quantum mechanics and quantum optics, such as the parametric down-conversion and the HOM interference at the microwave scales. Among other technical uses, our platform can Raman amplify an incoming signal preserving the wave vector, it can generate maximally entangled state, and it can be exploited in the framework of quantum thermodynamics as a quantum heat engine.

As extensions of this work we envisage the realization of chains of hybrid metamaterial TLs in which we can control the spectral feature of the propagating quanta with higher precision. In the framework of quantum metrology, this platform can find application in the realization of circuit versions of well-known interference platforms, such us collinear Mach-Zehnder and SU(1,1) interferometers. This work paves the way for future theoretical and experimental implementations of hybrid metamaterial transmission lines working at the quantum scales.

ACKNOWLEDGMENTS

The authors thank David Edward Bruschi for the helpful comments. The authors acknowledge support from the joint Project No. 13N15685 “German Quantum Computer based on Superconducting Qubits (GeQCoS)” sponsored by the German Federal Ministry of Education and Research (BMBF) under the framework “Quantum technologies–from basic research to the market.”

APPENDIX: HAMILTONIAN OF THE HYBRID TRANSMISSION LINE

In this section we want to discuss the derivation of our Hamiltonian, as well as the single contribution to the interaction Hamiltonian, in more details. We start from the linearized Lagrangian in Eqs. (2a), (2b), and (3). By means of the Legendre transformation,

$$\mathcal{H} = \sum_n \left(\frac{\partial\mathcal{L}}{\partial\dot{\Phi}_n^{\mathrm{L}}}\dot{\Phi}_n^{\mathrm{L}} + \frac{\partial\mathcal{L}}{\partial\dot{\Phi}_n^{\mathrm{R}}}\dot{\Phi}_n^{\mathrm{R}}\right) - \mathcal{L}, \tag{A1}$$

we obtain the total Hamiltonian

$$\hat{\mathcal{H}} = \hat{\mathcal{H}}_{\mathrm{L}} + \hat{\mathcal{H}}_{\mathrm{R}} + \hat{\mathcal{H}}_{\mathrm{I}}, \tag{A2}$$

where

$$\mathcal{H}_{\mathrm{L}} = \frac{1}{2}\sum_{n_{\mathrm{l}}=1}^{N}\left[\sum_{i=1}^{n_{\mathrm{l}}}\frac{(P_{n_{\mathrm{l}}}^{\mathrm{L}})^2}{C_{\mathrm{l}}} + \frac{(\Phi_{n_{\mathrm{l}}}^{\mathrm{L}})^2}{L_{\mathrm{l}}}\right] \tag{A3}$$

$$\mathcal{H}_{\mathrm{R}} = \frac{1}{2}\sum_{n_{\mathrm{r}}=1}^{N}\left[C_{\mathrm{r}}(P_{n_{\mathrm{r}}}^{\mathrm{R}})^2 + \frac{(\Phi_{n_{\mathrm{r}}+1}^{\mathrm{R}} - \Phi_{n_{\mathrm{r}}}^{\mathrm{R}})^2}{L_{\mathrm{r}}}\right] \tag{A4}$$

$$\mathcal{H}_{\mathrm{I}} = \frac{E(t)}{2}\left(\frac{2\pi}{\phi_0}\right)^2\left(\Phi_1^{\mathrm{L}} - \Phi_1^{\mathrm{R}}\right)^2, \tag{A5}$$

with conjugated momenta

$$P^{\mathrm{L}}_{n_{\mathrm{l}}} = \frac{\partial \mathcal{L}^{\mathrm{L}}}{\partial \dot{\Phi}_{n_{\mathrm{l}}}} = C_{\mathrm{l}} \left(2\dot{\Phi}^{\mathrm{L}}_{n_{\mathrm{l}}} - \dot{\Phi}^{\mathrm{L}}_{n_{\mathrm{l}}+1} - \dot{\Phi}^{\mathrm{L}}_{n_{\mathrm{l}}-1} \right)$$
$$= -i \sum_{|j|=1}^{N/2} W_j \left(e^{i(k_j n_{\mathrm{l}} \Delta x - \omega_j t)} a_j - \mathrm{h.c.} \right), \tag{A6}$$

$$P^{\mathrm{R}}_{n_{\mathrm{r}}} = \frac{\partial \mathcal{L}^{\mathrm{R}}}{\partial \dot{\Phi}_{n_{\mathrm{r}}}} = C_{\mathrm{r}} \dot{\Phi}^{\mathrm{R}}_{n_{\mathrm{r}}}$$
$$= -i \sum_{|j|=1}^{N/2} \sqrt{\frac{\hbar C_{\mathrm{r}} \upsilon_j}{2N}} \left(e^{i(p_j n_{\mathrm{r}} \Delta x - \upsilon_j t)} b_j - \mathrm{h.c.} \right), \tag{A7}$$

with $W_j = \sqrt{8\hbar C_{\mathrm{l}} \omega_j / (N)} \sin^2 \left(k_j \Delta x / 2 \right)$, where in the last lines we made use of the mode decomposition of the magnetic flux fields in Eqs. (5) and (6). Substituting the fields and the canonical momenta in Eqs. (5), (6), (A6), and (A7) into the Hamiltonian in Eq. (A2), summing with respect to the spatial indices n_{l} and n_{r}, and exploiting the commutation relations in Eqs. (10) and (11), we obtain the Hamiltonian contributions in Eqs. (12), (13), and (14).

Once we expand the square of the interaction Hamiltonian in Eq. (14), we distinguish the single contributions to the interaction, as done in Eq. (16). In what follows, we will present the explicit form of the single terms in Eq. (16) and describe their role in the dynamics.

The first term we want to present is

$$\hat{\mathcal{H}}_{\mathrm{ES}} = \frac{\hbar E(t)}{N} \left(\frac{2\pi}{\phi_0} \right)^2 \sum_{|j|=1}^{N/2} \left(\frac{1}{C_{\mathrm{l}} \omega_j} a^\dagger_j \hat{a}_j + \frac{1}{C_{\mathrm{r}} \upsilon_j} \hat{b}^\dagger_j \hat{b}_j \right). \tag{A8}$$

It describes the shift of the bare frequencies of the CTL, as discussed in Sec. III.

The interaction Hamiltonian describes both internal couplings, namely the interactions within the same TL, and external couplings, in which modes from the LHTL and the RHTL interact with each other. We now focus on the internal coupling terms, starting from

$$\hat{\mathcal{H}}_{\mathrm{RM}} = 2\chi(t) \sum_{\substack{i,j \\ i \neq j}}^{N/2} \left[\frac{1}{C_{\mathrm{l}} \sqrt{\omega_i \omega_j}} \hat{a}_i \hat{a}^\dagger_j e^{i(k_i - k_j)\Delta x} + \frac{1}{C_{\mathrm{r}} \sqrt{\upsilon_i \upsilon_j}} \hat{b}_i \hat{b}^\dagger_j e^{i(p_i - p_j)\Delta x} \right]. \tag{A9}$$

This contribution to the Hamiltonian is related to the internal Raman effect. Indeed, it describes the possibility to annihilate one particle and generate another particle with a different energy, depending on whether the TL absorbs from or releases energy to the SQUID. Clearly, the activation of this effect strongly depends on the time dependence of the Josephson energy at the SQUID.

The next two terms include the possibility to squeeze the state of a single TL by tuning the time-dependent Josephson energy. In particular,

$$\hat{\mathcal{H}}_{\mathrm{1S}} = \chi(t) \sum_{|j|=1}^{N/2} \left[\frac{1}{C_{\mathrm{l}} \omega_j} \hat{a}^2_j e^{2ik_j \Delta x} + \frac{1}{C_{\mathrm{r}} \upsilon_j} \hat{b}^2_j e^{2ip_j \Delta x} + \mathrm{h.c.} \right] \tag{A10}$$

describes the squeezing of a single mode of the CTL, generating therefore pairs of excitations within the same mode, whereas

$$\hat{\mathcal{H}}_{\mathrm{2S}} = \chi(t) \sum_{i,j}^{N/2} \left[\frac{1}{C_{\mathrm{l}} \sqrt{\omega_i \omega_j}} \hat{a}_i \hat{a}_j e^{i(k_i + k_j)\Delta x} + \frac{1}{C_{\mathrm{r}} \sqrt{\upsilon_i \upsilon_j}} \hat{b}_i \hat{b}_j e^{i(p_i + p_j)\Delta x} + \mathrm{h.c.} \right], \tag{A11}$$

describes the two-mode squeezing, namely the creation of two excitations in two different modes of the same TL.

Finally, we present the two external coupling terms, which have key implications in the interaction between the LHTL and the RHTL, and for this reason are largely discussed in the main text. As first, we introduce the hopping effect, associated with the Hamiltonian contribution

$$\hat{\mathcal{H}}_{\mathrm{HP}} = \frac{\chi(t)}{\sqrt{C_{\mathrm{l}} C_{\mathrm{r}}}} \sum_{i,j}^{N/2} \frac{1}{\sqrt{\omega_i \upsilon_j}} \left(\hat{a}_i \hat{b}^\dagger_j e^{i(k_i - p_j)\Delta x} + \mathrm{h.c.} \right). \tag{A12}$$

This term allows the propagation of excitations from one TL to the other one. Thanks to the time dependence of the Josephson energy, the hopping effect can occur also between modes having different energies. In this case, this effect corresponds to an external Raman scattering.

To conclude, the last contribution to the Hamiltonian is

$$\hat{\mathcal{H}}_{\mathrm{IS}} = -\frac{\hbar E(t)}{N \sqrt{C_{\mathrm{l}} C_{\mathrm{r}}}} \left(\frac{2\pi}{\phi_0} \right)^2 \sum_{i,j}^{N/2} \frac{1}{\sqrt{\omega_i \upsilon_j}} \left(a^\dagger_i \hat{b}^\dagger_j + \hat{a}_i \hat{b}_j \right). \tag{A13}$$

This term implies the possibility to squeeze two modes stemming from two different TL.

[1] I. M. Georgescu, S. Ashhab, and F. Nori, Quantum simulation, Rev. Mod. Phys. **86**, 153 (2014).

[2] J. Q. You and F. Nori, Atomic physics and quantum optics using superconducting circuits, Nature **474**, 589 (2011).

[3] C. M. Wilson, T. Duty, M. Sandberg, F. Persson, V. Shumeiko, and P. Delsing, Photon generation in an electromagnetic cavity with a time-dependent boundary, Phys. Rev. Lett. **105**, 233907 (2010).

[4] C. M. Wilson, G. Johansson, A. Pourkabirian, M. Simoen, J. R. Johansson, T. Duty, F. Nori, and P. Delsing, Observation of the dynamical Casimir effect in a superconducting circuit, Nature **479**, 376 (2011).

[5] J. Steinhauer, Observation of quantum hawking radiation and its entanglement in an analogue black hole, Nat. Phys. **12**, 959 (2016).

[6] P. O. Fedichev and U. R. Fischer, "Cosmological" quasiparticle production in harmonically trapped superfluid gases, Phys. Rev. A **69**, 033602 (2004).

[7] J. R. Muñoz De Nova, K. Golubkov, V. I. Kolobov, and J. Steinhauer, Observation of thermal Hawking radiation and its temperature in an analogue black hole, Nature **569**, 688 (2019).

[8] Y.-H. Shi, R.-Q. Yang, Z. Xiang, Z.-Y. Ge, H. Li, Y.-Y. Wang, K. Huang, Y. Tian, X. Song, D. Zheng, K. Xu, R.-G. Cai, and H. Fan, Quantum simulation of Hawking radiation and curved spacetime with a superconducting on-chip black hole, Nat. Commun. **14**, 3263 (2023).

[9] R. Casadio, A. Giugno, O. Micu, and A. Orlandi, Thermal BEC black holes, Entropy **17**, 6893 (2015).

[10] E. Altman *et al.*, Quantum simulators: Architectures and opportunities, PRX Quantum **2**, 017003 (2021).

[11] D. Marcos, P. Rabl, E. Rico, and P. Zoller, Superconducting circuits for quantum simulation of dynamical gauge fields, Phys. Rev. Lett. **111**, 110504 (2013).

[12] S. A. Wilkinson and M. J. Hartmann, Superconducting quantum many-body circuits for quantum simulation and computing, Appl. Phys. Lett. **116**, 230501 (2020).

[13] R. Barends, L. Lamata, J. Kelly, L. García-Álvarez, A. G. Fowler, A. Megrant, E. Jeffrey, T. C. White, D. Sank, and J. Y. Mutus *et al.*, Digital quantum simulation of fermionic models with a superconducting circuit, Nat. Commun. **6**, 7654 (2015).

[14] I. Buluta and F. Nori, Quantum simulators, Science **326**, 108 (2009).

[15] M. H. Devoret and R. J. Schoelkopf, Superconducting circuits for quantum information: An outlook, Science **339**, 1169 (2013).

[16] U. Vool and M. Devoret, Introduction to quantum electromagnetic circuits, Int. J. Circuit Theory Appl. **45**, 897 (2017).

[17] G. Wendin, Quantum information processing with superconducting circuits: A review, Rep. Prog. Phys. **80**, 106001 (2017).

[18] O. Kyriienko and A. S. Sørensen, Floquet quantum simulation with superconducting qubits, Phys. Rev. Appl. **9**, 064029 (2018).

[19] S. Raeisi, N. Wiebe, and B. C. Sanders, Quantum-circuit design for efficient simulations of many-body quantum dynamics, New J. Phys. **14**, 103017 (2012).

[20] Z.-L. Xiang, S. Ashhab, J. Q. You, and F. Nori, Hybrid quantum circuits: Superconducting circuits interacting with other quantum systems, Rev. Mod. Phys. **85**, 623 (2013).

[21] S. Fedortchenko, S. Felicetti, D. Marković, S. Jezouin, A. Keller, T. Coudreau, B. Huard, and P. Milman, Quantum simulation of ultrastrongly coupled bosonic modes using superconducting circuits, Phys. Rev. A **95**, 042313 (2017).

[22] A. A. Houck, H. E. Türeci, and J. Koch, On-chip quantum simulation with superconducting circuits, Nat. Phys. **8**, 292 (2012).

[23] J. J. García-Ripoll, E. Solano, and M. A. Martin-Delgado, Quantum simulation of Anderson and Kondo lattices with superconducting qubits, Phys. Rev. B **77**, 024522 (2008).

[24] F. Mei, V. M. Stojanović, I. Siddiqi, and L. Tian, Analog superconducting quantum simulator for Holstein polarons, Phys. Rev. B **88**, 224502 (2013).

[25] J. K. Nauth and V. M. Stojanović, Spectral features of polaronic excitations in a superconducting analog simulator, Phys. Rev. B **107**, 174306 (2023).

[26] V. M. Stojanović and I. Salom, Quantum dynamics of the small-polaron formation in a superconducting analog simulator, Phys. Rev. B **99**, 134308 (2019).

[27] V. M. Stojanović, M. Vanević, E. Demler, and L. Tian, Transmon-based simulator of nonlocal electron-phonon coupling: A platform for observing sharp small-polaron transitions, Phys. Rev. B **89**, 144508 (2014).

[28] A. Blais, A. L. Grimsmo, S. Girvin, and A. Wallraff, Circuit quantum electrodynamics, Rev. Mod. Phys. **93**, 025005 (2021).

[29] A. Blais, R.-S. Huang, A. Wallraff, S. M. Girvin, and R. J. Schoelkopf, Cavity quantum electrodynamics for superconducting electrical circuits: An architecture for quantum computation, Phys. Rev. A **69**, 062320 (2004).

[30] A. M. Zagoskin, E. Il'ichev, M. W. McCutcheon, J. F. Young, and F. Nori, Controlled generation of squeezed states of microwave radiation in a superconducting resonant circuit, Phys. Rev. Lett. **101**, 253602 (2008).

[31] J. Zhang, R. Ferguson, S. Kühn, J. F. Haase, C. Wilson, K. Jansen, and C. A. Muschik, Simulating gauge theories with variational quantum eigensolvers in superconducting microwave cavities, Quantum **7**, 1148 (2023).

[32] L.-H. Du, J. Q. You, and L. Tian, Superconducting circuit probe for analog quantum simulators, Phys. Rev. A **92**, 012330 (2015).

[33] B. Yurke and J. S. Denker, Quantum network theory, Phys. Rev. A **29**, 1419 (1984).

[34] N. D. Birrell and P. C. W. Davies, *Quantum Fields in Curved Space* (Cambridge University Press, Cambridge, UK, 1984).

[35] P. D. Nation, J. R. Johansson, M. P. Blencowe, and F. Nori, *Colloquium*: Stimulating uncertainty: Amplifying the quantum vacuum with superconducting circuits, Rev. Mod. Phys. **84**, 1 (2012).

[36] Z. Tian, J. Jing, and A. Dragan, Analog cosmological particle generation in a superconducting circuit, Phys. Rev. D **95**, 125003 (2017).

[37] S. Lang and R. Schützhold, Analog of cosmological particle creation in electromagnetic waveguides, Phys. Rev. D **100**, 065003 (2019).

[38] P. Lähteenmäki, G. S. Paraoanu, J. Hassel, and P. J. Hakonen, Dynamical Casimir effect in a Josephson metamaterial, Proc. Natl. Acad. Sci. **110**, 4234 (2013).

[39] J. R. Johansson, G. Johansson, C. M. Wilson, and F. Nori, Dynamical Casimir effect in a superconducting coplanar waveguide, Phys. Rev. Lett. **103**, 147003 (2009).
[40] J. R. Johansson, G. Johansson, C. M. Wilson, and F. Nori, Dynamical Casimir effect in superconducting microwave circuits, Phys. Rev. A **82**, 052509 (2010).
[41] S. S. Kadijani, N. Del Grosso, T. L. Schmidt, and M. B. Farias, Dynamical Casimir cooling in circuit QED systems, Phys. Rev. B **109**, 245417 (2024).
[42] P. D. Nation, M. P. Blencowe, A. J. Rimberg, and E. Buks, Analogue Hawking radiation in a dc-SQUID array transmission line, Phys. Rev. Lett. **103**, 087004 (2009).
[43] Z. Tian and J. Du, Analogue Hawking radiation and quantum soliton evaporation in a superconducting circuit, The European Physical Journal C **79**, 994 (2019).
[44] M. P. Blencowe and H. Wang, Analogue gravity on a superconducting chip, Philos. Trans. R. Soc., A: Math. Phys. Eng. Sci. **378**, 20190224 (2020).
[45] Y.-H. Shi, R.-Q. Yang, Z. Xiang, Z.-Y. Ge, H. Li, Y.-Y. Wang, K. Huang, Y. Tian, X. Song, and D. Zheng *et al.*, Quantum simulation of Hawking radiation and curved spacetime with a superconducting on-chip black hole, Nat. Commun. **14**, 3263 (2023).
[46] V. G. Veselago, Electrodynamics of substances with simultaneously negative and, Usp. fiz. Nauk **92**, 517 (1967).
[47] D. R. Smith, W. J. Padilla, D. C. Vier, S. C. Nemat-Nasser, and S. Schultz, Composite medium with simultaneously negative permeability and permittivity, Phys. Rev. Lett. **84**, 4184 (2000).
[48] D. R. Smith and N. Kroll, Negative refractive index in left-handed materials, Phys. Rev. Lett. **85**, 2933 (2000).
[49] A. A. Houck, J. B. Brock, and I. L. Chuang, Experimental observations of a left-handed material that obeys Snell's law, Phys. Rev. Lett. **90**, 137401 (2003).
[50] A. B. Kozyrev and D. W. Van Der Weide, Nonlinear left-handed transmission line metamaterials, J. Phys. D: Appl. Phys. **41**, 173001 (2008).
[51] A. Ferreri, D. E. Bruschi, and F. K. Wilhelm, Particle creation in left-handed metamaterial transmission lines, Phys. Rev. Res. **6**, 033204 (2024).
[52] T. McBroom-Carroll, A. Schlabes, X. Xu, J. Ku, B. Cole, S. Indrajeet, M. D. LaHaye, M. H. Ansari, and B. L. T. Plourde, Entangling interactions between artificial atoms mediated by a multimode left-handed superconducting ring resonator, PRX Quantum **5**, 020325 (2024).
[53] C. Caloz, A. Sanada, and T. Itoh, A novel composite right-/left-handed coupled-line directional coupler with arbitrary coupling level and broad bandwidth, IEEE Trans. Microw. Theory Tech. **52**, 980 (2004).
[54] D. J. Egger and F. K. Wilhelm, Multimode circuit quantum electrodynamics with hybrid metamaterial transmission lines, Phys. Rev. Lett. **111**, 163601 (2013).
[55] A. Messinger, B. G. Taketani, and F. K. Wilhelm, Left-handed superlattice metamaterials for circuit QED, Phys. Rev. A **99**, 032325 (2019).
[56] H. Wang, A. Zhuravel, S. Indrajeet, B. Taketani, M. Hutchings, Y. Hao, F. Rouxinol, F. Wilhelm, M. LaHaye, A. Ustinov, and B. Plourde, Mode structure in superconducting metamaterial transmission-line resonators, Phys. Rev. Appl. **11**, 054062 (2019).
[57] A. A. Gangat, I. P. McCulloch, and G. J. Milburn, Deterministic many-resonator *w* entanglement of nearly arbitrary microwave states via attractive Bose-Hubbard simulation, Phys. Rev. X **3**, 031009 (2013).
[58] V. M. Stojanović, Bare-excitation ground state of a spinless-fermion–boson model and *w*-state engineering in an array of superconducting qubits and resonators, Phys. Rev. Lett. **124**, 190504 (2020).
[59] S. Vinjanampathy and J. Anders, Quantum thermodynamics, Contemp. Phys. **57**, 545 (2016).
[60] R. Kosloff, Quantum thermodynamics: A dynamical viewpoint, Entropy **15**, 2100 (2013).
[61] J. P. Pekola, Towards quantum thermodynamics in electronic circuits, Nat. Phys. **11**, 118 (2015).
[62] T. Weißl, B. Küng, E. Dumur, A. K. Feofanov, I. Matei, C. Naud, O. Buisson, F. W. J. Hekking, and W. Guichard, Kerr coefficients of plasma resonances in Josephson junction chains, Phys. Rev. B **92**, 104508 (2015).
[63] C. K. Law, Interaction between a moving mirror and radiation pressure: A Hamiltonian formulation, Phys. Rev. A **51**, 2537 (1995).
[64] A. Ferreri, H. Pfeifer, F. K. Wilhelm, S. Hofferberth, and D. E. Bruschi, Interplay between optomechanics and the dynamical Casimir effect, Phys. Rev. A **106**, 033502 (2022).
[65] A. Ferreri, Quantum vibrational mode in a cavity confining a massless spinor field, Phys. Rev. A **106**, 052204 (2022).
[66] W. H. Louisell, *Quantum Statistical Properties of Radiation* (John Wiley and Sons, Inc., New York, 1973).
[67] M. Islam, Raman amplifiers for telecommunications, IEEE J. Sel. Top. Quantum Electron. **8**, 548 (2002).
[68] L.-A. Wu, H. J. Kimble, J. L. Hall, and H. Wu, Generation of squeezed states by parametric down conversion, Phys. Rev. Lett. **57**, 2520 (1986).
[69] J. G. Rarity, P. R. Tapster, and E. Jakeman, Observation of sub-poissonian light in parametric downconversion, Opt. Commun. **62**, 201 (1987).
[70] M. H. Rubin, D. N. Klyshko, Y. H. Shih, and A. V. Sergienko, Theory of two-photon entanglement in type-ii optical parametric down-conversion, Phys. Rev. A **50**, 5122 (1994).
[71] A. Christ, B. Brecht, W. Mauerer, and C. Silberhorn, Theory of quantum frequency conversion and type-ii parametric down-conversion in the high-gain regime, New J. Phys. **15**, 053038 (2013).
[72] M. O. Scully and M. S. Zubairy, *Quantum Optics* (American Association of Physics Teachers, Cambridge, UK, 1999).
[73] C. K. Hong, Z. Y. Ou, and L. Mandel, Measurement of subpicosecond time intervals between two photons by interference, Phys. Rev. Lett. **59**, 2044 (1987).
[74] K. Mattle, H. Weinfurter, P. G. Kwiat, and A. Zeilinger, Dense coding in experimental quantum communication, Phys. Rev. Lett. **76**, 4656 (1996).
[75] F. Bouchard, A. Sit, Y. Zhang, R. Fickler, F. M. Miatto, Y. Yao, F. Sciarrino, and E. Karimi, Two-photon interference: the Hong–Ou–Mandel effect, Rep. Prog. Phys. **84**, 012402 (2021).
[76] K.-H. Luo, M. Santandrea, M. Stefszky, J. Sperling, M. Massaro, A. Ferreri, P. R. Sharapova, H. Herrmann, and C. Silberhorn, Quantum optical coherence: From linear

to nonlinear interferometers, Phys. Rev. A **104**, 043707 (2021).
[77] M. S. Abdalla, The statistical properties of a generalized two-mode squeezed operator, J. Mod. Opt. **39**, 1067 (1992).
[78] D. E. Bruschi, G. S. Paraoanu, I. Fuentes, F. K. Wilhelm, and A. W. Schell, General solution of the time evolution of two interacting harmonic oscillators, Phys. Rev. A **103**, 023707 (2021).
[79] P. Forn-Díaz, L. Lamata, E. Rico, J. Kono, and E. Solano, Ultrastrong coupling regimes of light-matter interaction, Rev. Mod. Phys. **91**, 025005 (2019).
[80] M.-A. Lemonde, N. Didier, and A. A. Clerk, Nonlinear Interaction Effects in a Strongly Driven Optomechanical Cavity, Phys. Rev. Lett. **111**, 053602 (2013).
[81] H. T. Quan, Y. D. Wang, Y.-x. Liu, C. P. Sun, and F. Nori, Maxwell's Demon assisted thermodynamic cycle in superconducting quantum circuits, Phys. Rev. Lett. **97**, 180402 (2006).
[82] N. F. Del Grosso, F. C. Lombardo, F. D. Mazzitelli, and P. I. Villar, Quantum Otto cycle in a superconducting cavity in the nonadiabatic regime, Phys. Rev. A **105**, 022202 (2022).
[83] R. Kosloff and A. Levy, Quantum heat engines and refrigerators: Continuous devices, Annu. Rev. Phys. Chem. **65**, 365 (2014).
[84] A. Ferreri, V. Macrì, F. K. Wilhelm, F. Nori, and D. E. Bruschi, Quantum field heat engine powered by phonon-photon interactions, Phys. Rev. Res. **5**, 043274 (2023).
[85] A. Levy and R. Kosloff, Quantum absorption refrigerator, Phys. Rev. Lett. **108**, 070604 (2012).
[86] E. A. Martinez and J. P. Paz, Dynamics and thermodynamics of linear quantum open systems, Phys. Rev. Lett. **110**, 130406 (2013).
[87] R. Grobe, K. Rzazewski, and J. H. Eberly, Measure of electron-electron correlation in atomic physics, J. Phys. B: At., Mol. Opt. Phys. **27**, L503 (1994).
[88] C. K. Law, I. A. Walmsley, and J. H. Eberly, Continuous frequency entanglement: Effective finite Hilbert space and entropy control, Phys. Rev. Lett. **84**, 5304 (2000).
[89] C. K. Law and J. H. Eberly, Analysis and interpretation of high transverse entanglement in optical parametric down conversion, Phys. Rev. Lett. **92**, 127903 (2004).
[90] S. Lemieux, M. Manceau, P. R. Sharapova, O. V. Tikhonova, R. W. Boyd, G. Leuchs, and M. V. Chekhova, Engineering the frequency spectrum of bright squeezed vacuum via group velocity dispersion in an SU(1,1) interferometer, Phys. Rev. Lett. **117**, 183601 (2016).
[91] P. Sharapova, A. M. Pérez, O. V. Tikhonova, and M. V. Chekhova, Schmidt modes in the angular spectrum of bright squeezed vacuum, Phys. Rev. A **91**, 043816 (2015).
[92] A. Christ, K. Laiho, A. Eckstein, K. N. Cassemiro, and C. Silberhorn, Probing multimode squeezing with correlation functions, New J. Phys. **13**, 033027 (2011).
[93] Y. Jeronimo-Moreno and A. B. U'Ren, Control, measurement, and propagation of entanglement in photon pairs generated through type-ii parametric down-conversion, Phys. Rev. A **79**, 033839 (2009).
[94] In what follows, we will not write the exact form of the coupling parameters contained in each term of Eq. (59). To check the order of magnitude of these effects it suffices to know that each coupling parameter is proportional to

$$\xi \propto \sqrt{\frac{L_r L_1}{C_r C_1}} \frac{E(t)}{N^2} \left(\frac{2\pi}{\phi_0}\right)^4,$$

where we have written the explicit time dependence of the Josephson energy. We recall that effects mediated by the modulation of the Josephson energy have a coupling parameter proportional to

$$\xi \propto \sqrt{\frac{L_r L_1}{C_r C_1}} \frac{\eta E_0}{N^2} \left(\frac{2\pi}{\phi_0}\right)^4.$$

[95] Y. Krupko, V. D. Nguyen, T. Weißl, E. Dumur, J. Puertas, R. Dassonneville, C. Naud, F. W. J. Hekking, D. M. Basko, O. Buisson, N. Roch, and W. Hasch-Guichard, Kerr nonlinearity in a superconducting Josephson metamaterial, Phys. Rev. B **98**, 094516 (2018).
[96] E. Russo, A. Mercurio, F. Mauceri, R. Lo Franco, F. Nori, S. Savasta, and V. Macrì, Optomechanical two-photon hopping, Phys. Rev. Res. **5**, 013221 (2023).